

Global Fits of Third Family Hypercharge Models to Neutral Current B-Anomalies and Electroweak Precision Observables

B.C. Allanach¹, J. Eliel Camargo-Molina², and Joe Davighi¹

¹ DAMTP, University of Cambridge, Wilberforce Road, Cambridge, CB3 0WA, United Kingdom

² Department of Physics and Astronomy, Uppsala University, Box 516, SE-751 20 Uppsala, Sweden

Received: date / Accepted: date

Abstract. While it is known that third family hypercharge models can explain the neutral current B -anomalies, it was hitherto unclear whether the $Z - Z'$ mixing predicted by such models could simultaneously fit electroweak precision observables. Here, we perform global fits of several third family hypercharge models to a combination of electroweak data and those data pertinent to the neutral current B -anomalies. While the Standard Model is in tension with this combined data set with a p -value of .00068, simple versions of the models (fitting two additional parameters each) provide much improved fits.

The original Third Family Hypercharge Model, for example, has a p -value of .065, with $\sqrt{\Delta\chi^2} = 6.5\sigma$.

1 Introduction

The neutral current B -anomalies (NCBAs) consist of various measurements in hadronic particle decays which, collectively, are in tension with Standard Model (SM) predictions. The particular observables displaying such tension often involve an effective vertex with an anti-bottom quark, a strange quark, a muon and an anti-muon, *i.e.* $(\bar{b}s)(\mu^+\mu^-)$, plus the charge conjugated version. Observables such as the ratios of branching ratios $R_K^{(*)} = BR(B \rightarrow K^{(*)}\mu^+\mu^-)/BR(B \rightarrow K^{(*)}e^+e^-)$ are not displaying the lepton flavour universality (LFU) property expected of the SM [1–3]. Such observables are of particular interest because much of the theoretical uncertainty in the prediction cancels in the ratio, leaving the prediction rather precise. Other NCBA observables display some disparity with SM predictions even when their larger theoretical uncertainties are taken into account, for example $BR(B_s \rightarrow \mu^+\mu^-)$ [4–8], $BR(B_s \rightarrow \phi\mu^+\mu^-)$ [9, 10] and angular distributions of $B \rightarrow K^{(*)}\mu^+\mu^-$ decays [11–16]. Global fits find that new physics contributions to the $(\bar{b}s)(\mu^+\mu^-)$ effective vertex can fit the NCBAs much better than the SM can [17–23].

A popular option for beyond the SM (BSM) explanations of the NCBAs is that of a Z' vector boson with family dependent interactions [24–28]. Such a particle is predicted by models with a BSM spontaneously broken $U(1)$ gauged flavour symmetry. The additional quantum numbers of the SM fermions are constrained by the need to cancel local anomalies [29–31], for example muon minus tau lepton number [32–37], third family baryon number minus second family lepton number [38–40], third family hypercharge [41–43] or other assignments [44–62].

The current paper is about the third family hypercharge option. The Third Family Hypercharge Model [41] (henceforth abbreviated as the ‘ Y_3 model’) explains the hierarchical heaviness of the third family and the smallness of quark mixing. It was shown to successfully fit NCBAs, along with constraints from $B_s - \bar{B}_s$ mixing and LFU constraints on Z^0 boson interactions. The ATLAS experiment at the LHC has searched¹ for the production of BSM resonances that yield a peak in the di-muon invariant mass ($m_{\mu\mu}$) spectrum, but have yet to find a significant one [64]. This implies a lower bound upon the mass of the Z' in the Y_3 model, $M_X > 1.2$ TeV [65], but plenty of viable parameter space remains which successfully explains the NCBAs. A variant, the Deformed Third Family Hypercharge Model (DY₃ model), was subsequently introduced [43] in order to remedy a somewhat ugly feature (ugly from a naturalness point of view) in the construction of the original Y_3 model: namely, that a Yukawa coupling allowed at the renormalisable level was assumed to be tiny in order to agree with strict lepton flavour violation constraints. The DY₃ model can simultaneously fit the NCBAs and be consistent with the ATLAS di-muon direct search constraint for $1.2 \text{ TeV} < M_X < 12 \text{ TeV}$. We will also present results for a third variant, the DY_{3}' model, which is identical to the DY₃ model but with charges for second and third family leptons interchanged. As we show later on, this results in a better fit to data due to the different helicity structure of the couplings of the Z' boson to muons (see section 4.3 for details).}

¹ During the final stages of preparation of this manuscript, the CMS experiment released a di-muon resonance search [63] with similar exclusion regions.

In either of these third family hypercharge models, the local gauge symmetry of the SM is² extended to $SU(3) \times SU(2) \times U(1)_Y \times U(1)_X$. This is spontaneously broken to the SM gauge group by the non-zero vacuum expectation value (VEV) of a SM-singlet ‘flavon’ field θ that has a non-zero $U(1)_X$ charge. In each model, the third family quarks’ $U(1)_X$ charges are equal to their hypercharges whereas the first two family quarks are chargeless under $U(1)_X$. We must (since it is experimentally determined to be $\mathcal{O}(1)$ and is therefore inconsistent with a suppressed, non-renormalisable coupling) ensure that a renormalisable top Yukawa coupling is allowed by $U(1)_X$; this implies that the SM Higgs doublet field should have $U(1)_X$ charge equal to its hypercharge. Consequently, when the Higgs doublet acquires a VEV to break the electroweak symmetry, this gives rise to $Z^0 - Z'$ mixing [41]. Such mixing is subject to stringent constraints from electroweak precision observables (EWPOs), in particular from the ρ -parameter, which encodes the ratio of the masses of the Z^0 boson and the W boson [66].

Third family hypercharge models can fit the NCBA’s for a range of the ratio of the Z' gauge coupling to its mass g_X/M_X which does *not* contain zero. This means that it is not possible to ‘tune the $Z - Z'$ mixing away’ if one wishes the model to fit the NCBA’s. As a consequence, it is not clear whether the EWPOs will strongly preclude the (D) Y_3 models from explaining the NCBA’s or not.

The purpose of this paper is to perform a global fit to a combined set of electroweak and NCBA-type data, along with other relevant constraints on flavour changing neutral currents (FCNCs). It is clear that the SM provides a poor fit to this combined set, as Table 1 shows. A p -value³ of .00068 corresponds to ‘tension at the 3.4σ level’. The (D) Y_3 models are of particular interest as plausible models of new physics if they fit the data significantly better than the SM, a question which can best be settled by performing appropriate global fits.

Our paper proceeds as follows: we introduce the models and define their parameter spaces in §2. At renormalisation scales at or below M_X but above M_W , we encode the new physics effects in each model via the Standard Model Effective Theory (SMEFT). We calculate the leading (dimension-6) SMEFT operators predicted by our models at the scale M_X in §3. These provide the input to the calculation of observables by `smelli-2.2.0` [67]⁴, which we describe at the beginning of §4. The results of

data set	χ^2	n	p -value
quarks	221.2	167	.0032
LFU FCNCs	35.3	21	.026
EWPOs	35.7	31	.26
global	292.2	219	.00068

Table 1. SM goodness of fit for the different data sets we consider, as calculated by `smelli-2.2.0`. We display the total Pearson’s chi-squared χ^2 for each data set along with the number of observables n and the data set’s p -value. The set named ‘quarks’ contains $BR(B_s \rightarrow \phi\mu^+\mu^-)$, $BR(B_s \rightarrow \mu^+\mu^-)$, Δm_s and various differential distributions in $B \rightarrow K^{(*)}\mu^+\mu^-$ decays among others, whereas ‘LFU FCNCs’ contains $R_{K^{(*)}}$ and some B meson decay branching ratios into di-taus. Our sets are identical to those defined by `smelli-2.2.0` and we refer the curious reader to its manual [67], where the observables are enumerated. We have updated R_K and $BR(B_{s,d} \rightarrow \mu^+\mu^-)$ with the latest LHCb measurements as detailed in the text.

the fits are presented in the remainder of §4, before a discussion in §5.

2 Models

In this section we review the models of interest to this study, in sufficient detail so as to proceed with the calculation of the SMEFT Wilson coefficients (WCs) in the following section. Under $SU(3) \times SU(2) \times U(1)_Y$, we define the fermionic fields such that they transform in the following representations: $Q_{Li} := (u_{Li} \ d_{Li})^T \sim (\mathbf{3}, \mathbf{2}, +1/6)$, $L_{Li} := (\nu_{Li} \ e_{Li})^T \sim (\mathbf{1}, \mathbf{2}, -1/2)$, $e_{Ri} \sim (\mathbf{1}, \mathbf{1}, -1)$, $d_{Ri} \sim (\mathbf{3}, \mathbf{1}, -1/3)$, $u_{Ri} \sim (\mathbf{3}, \mathbf{1}, +2/3)$, where $i \in \{1, 2, 3\}$ is a family index ordered by increasing mass. Implicit in the definition of these fields is that we have performed a flavour rotation so that $d_{Li}, e_{Li}, e_{Ri}, d_{Ri}, u_{Ri}$ are mass basis fields. In what follows, we denote 3-component column vectors in family space with bold font, for example $\mathbf{u}_L := (u_L, c_L, t_L)^T$. The Higgs doublet is a complex scalar $\phi \sim (\mathbf{1}, \mathbf{2}, +1/2)$, and all three models which we consider (the Y_3 model, the DY_3 model and the DY_3' model) incorporate a complex scalar flavon with SM quantum numbers $\theta \sim (\mathbf{1}, \mathbf{1}, 0)$, which has a $U(1)_X$ charge $X_\theta \neq 0$ and is used to Higgs the $U(1)_X$ symmetry, such that its gauge boson acquires a mass at the TeV scale or higher.

In the following we will present our results for three variants of third family hypercharge models, which differ in the charge assignment for the SM fields:

- The Y_3 model, introduced in [41]. Only third generation fermions have non-zero $U(1)_X$ charges. The charge assignments can be read in Table 2.
- The DY_3 model as introduced in [43]. It differs from the Y_3 model in that charges have been assigned to the second generation leptons as well, while still being anomaly free.
- The DY_3' model, which differs from the DY_3 model in that the charges for third and second generation left-handed leptons are interchanged. The charge assignments can be read in Table 3.

² Possible quotients of the gauge group by discrete subgroups play no role in our argument and so we shall henceforward ignore them.

³ All χ^2 and p -values which we present here are calculated in `smelli-2.2.0`. We estimate that the numerical uncertainty in the `smelli-2.2.0` calculation of a global χ^2 value is ± 1 and the resulting uncertainty in the second significant figure of any global p -value quoted is ± 3 .

⁴ We use the development version of `smelli-2.2.0` that was released on `github` on 8th March 2021 which we have updated to take into account 2021 LHCb measurements of R_K , $BR(B_s \rightarrow \mu^+\mu^-)$ and $BR(B \rightarrow \mu^+\mu^-)$.

All three of these gauge symmetries have identical couplings to quarks, coupling only to the third family via hypercharge quantum numbers. This choice means that, of the quark Yukawa couplings, only the top and bottom Yukawa couplings are present at the renormalisable level. Of course, the light quarks are not massless in reality; their masses, as well as the small quark mixing angles, must be encoded in higher-dimensional operators that come from a further layer of heavy physics, such as a suite of heavy vector-like fermions at a mass scale $\Lambda > M_X/g_X$, where g_X is the $U(1)_X$ gauge coupling.

Whatever this heavy physics might be, the structure of the light quark Yukawa couplings will be governed by the size of parameters that break the $U(2)_{\text{global}}^3 := U(2)_q \times U(2)_u \times U(2)_d$ accidental global symmetry [68–72] of the renormalisable third family hypercharge lagrangians. For example, a minimal set of spurions charged under both $U(2)_{\text{global}}^3$ and $U(1)_X$ was considered⁵ in Ref. [73], which reproduces the observed hierarchies in quark masses and mixing angles when the scale Λ of new physics is a factor of 15 or so larger than M_X/g_X . Taking this hierarchy of scales as a general guide, and observing that the global fits to electroweak and flavour data that we perform in this paper prefer $M_X/g_X \approx 10$ TeV, we expect the new physics scale to be around $\Lambda \approx 150$ TeV. This scale is high enough to suppress most contributions of the heavy physics, about which we remain agnostic, to low energy phenomenology including precise flavour bounds⁶. For this reason, we feel safe in neglecting the contributions of the Λ scale physics to the SMEFT coefficients that we calculate in § 3, and shall not consider it in any further detail.

Continuing, we will first detail the scalar sector, which is common to (and identical in) all of the third family hypercharge models, before going on to discuss aspects of each model that are different (most importantly, the couplings to leptons).

2.1 The scalar sector

The coupling of the flavon to the $U(1)_X$ gauge field is encoded in the covariant derivative

$$D_\mu \theta = (\partial_\mu + iX_\theta g_X X_\mu) \theta, \quad (1)$$

where X_μ is the $U(1)_X$ gauge boson in the unbroken phase and g_X is its gauge coupling. The flavon θ is assumed to acquire a VEV $\langle \theta \rangle$ at (or above) the TeV scale, which spontaneously breaks $U(1)_X$. Expanding $\theta = (\langle \theta \rangle + \vartheta)/\sqrt{2}$, its kinetic terms $(D_\mu \theta)^\dagger D^\mu \theta$ in the Lagrangian density give the gauge boson a mass $M_X = X_\theta g_X \langle \theta \rangle$ through the

⁵ In the present paper we take a more phenomenological approach in specifying the fermion mixing matrices, but nonetheless, the quark mixing matrices that we use are qualitatively similar to those expected from the $U(2)_{\text{global}}^3 \times U(1)_X$ breaking spurion analysis. For example, there is no mixing in the right-handed fields.

⁶ Kaon mixing is one possible exception where such heavy physics might play a non-trivial role, however.

$X_{Q_i} = 0$	$X_{u_{R_i}} = 0$	$X_{d_{R_i}} = 0$
$X_{Q_3} = 1/6$	$X_{u_{R3}} = 2/3$	$X_{d_{R3}} = -1/3$
$X_{L_i} = 0$	$X_{e_{R_i}} = 0$	$X_\phi = 1/2$
$X_{L_3} = -1/2$	$X_{e_{R3}} = -1$	X_θ

Table 2. $U(1)_X$ charges of the gauge eigenbasis fields in the Y_3 model, where $i \in \{1, 2\}$. The flavon charge X_θ is left undetermined.

Higgs mechanism. After electroweak symmetry breaking, the electrically-neutral gauge bosons X , W^3 and B mix, giving rise to γ , Z^0 and Z' as the physical mass eigenstates [41]. To terms of order (M_Z^2/M_X^2) , the mass and the couplings of the X boson are equivalent to those of the Z' boson. Because we take $M_X \gg M_Z$, the matching to the SMEFT (§3) should be done in the unbroken electroweak phase, where it is the X boson that is properly integrated out. In the rest of this section we therefore specify the $U(1)_X$ sector via the X boson and its couplings. Throughout this paper, we entreat the reader to bear in mind that in terms of searches and several other aspects of their phenomenology, to a decent approximation the X boson and the Z' boson are synonymous.

The covariant derivative of the Higgs doublet is

$$D_\mu \phi = \left(\partial_\mu + i\frac{g}{2} \sigma^a W_\mu^a + i\frac{g'}{2} B_\mu + i\frac{g_X}{2} X_\mu \right) \phi, \quad (2)$$

where W_μ^a ($a = 1, 2, 3$) are unbroken $SU(2)$ gauge bosons, σ^a are the Pauli matrices, g is the $SU(2)$ gauge coupling, B_μ is the hypercharge gauge boson and g' is the hypercharge gauge coupling. The kinetic term for the Higgs field, $(D_\mu \phi)^\dagger (D^\mu \phi)$, contains terms both linear and quadratic in X_μ . It is the linear terms

$$\mathcal{L} \supset -i\frac{g_X}{2} X_\mu \phi^\dagger \left(\partial_\mu + i\frac{g}{2} \sigma^a W_\mu^a + i\frac{g'}{2} B_\mu \right) \phi + \text{h.c.} \quad (3)$$

that, upon integrating out the X_μ boson, will give the leading contribution to the SMEFT in the form of dimension-6 operators involving the Higgs, as we describe in §3.

The charges of the fermion fields differ between the Y_3 model and the DY'_3 model, as follows.

2.2 Fermion couplings: the Y_3 model

The Y_3 model has fermion charges as listed in Table 2 (in the gauge eigenbasis), leading to the following Lagrangian density describing the X boson-SM fermion couplings [41]:

$$\begin{aligned} \mathcal{L}_{Y_3}^\psi = & -g_X \left(\frac{1}{6} \overline{\mathbf{Q}}_{\mathbf{L}} \Lambda_\xi^{(d_L)} \not{X} \mathbf{Q}_{\mathbf{L}} - \frac{1}{2} \overline{\mathbf{L}}_{\mathbf{L}} \Lambda_\xi^{(e_L)} \not{X} \mathbf{L}_{\mathbf{L}} \right. \\ & + \frac{2}{3} \overline{\mathbf{u}}_{\mathbf{R}} \Lambda_\xi^{(u_R)} \not{X} \mathbf{u}_{\mathbf{R}} - \frac{1}{3} \overline{\mathbf{d}}_{\mathbf{R}} \Lambda_\xi^{(d_R)} \not{X} \mathbf{d}_{\mathbf{R}} \\ & \left. - \overline{\mathbf{e}}_{\mathbf{R}} \Lambda_\xi^{(e_R)} \not{X} \mathbf{e}_{\mathbf{R}} \right), \end{aligned} \quad (4)$$

where

$$A_P^{(I)} := V_I^\dagger P V_I \quad (5)$$

$X_{Q_1} = 0$	$X_{u_{R1}} = 0$	$X_{d_{R1}} = 0$
$X_{Q_2} = 0$	$X_{u_{R2}} = 0$	$X_{d_{R2}} = 0$
$X_{Q_3} = 1/6$	$X_{u_{R3}} = 2/3$	$X_{d_{R3}} = -1/3$
$X_{L_1} = 0$	$X_{e_{R1}} = 0$	$X_\phi = 1/2$
$X_{L_2} = -4/3$	$X_{e_{R2}} = 2/3$	X_θ
$X_{L_3} = 5/6$	$X_{e_{R3}} = -5/3$	

Table 3. $U(1)_X$ charges of the gauge eigenbasis fields in the DY'_3 model. The original DY_3 model charges (as introduced in Ref. [43]) can be obtained by interchanging X_{L_3} and X_{L_2} . The flavon charge X_θ is left undetermined.

are Hermitian 3-by-3 matrices. The index $I \in \{u_L, d_L, e_L, \nu_L, u_R, d_R, e_R\}$ and the matrix $P \in \{\xi, \Omega, \Psi\}$, where

$$\xi = \begin{pmatrix} 0 & 0 & 0 \\ 0 & 0 & 0 \\ 0 & 0 & 1 \end{pmatrix}, \quad (6)$$

and Ω and Ψ are described in §2.3. The V_I are 3-by-3 unitary matrices describing the mixing between fermionic gauge eigenstates and their mass eigenstates. Note that the quark doublets have been family rotated so that the d_{L_i} (but not the u_{L_i} fields) correspond to their mass eigenstates. Similarly, we have rotated L_i such that e_{L_i} align with the charged lepton mass eigenstates, but ν_{L_i} are not. This will simplify the matching to the SMEFT operators that we perform in §3. We now go on to cover the X boson couplings in the DY'_3 model before detailing the fermion mixing ansatz (which is common to all three models).

2.3 Fermion couplings: the DY'_3 model

For the DY'_3 model with the charge assignments listed in Table 3, the Lagrangian contains the following X boson-SM fermion couplings [43]:

$$\begin{aligned} \mathcal{L}_{DY'_3}^\psi = -g_X & \left(\frac{1}{6} \overline{\mathbf{Q}_L} \Lambda_\xi^{(d_L)} \not{X} \mathbf{Q}_L - \frac{4}{3} \overline{\mathbf{L}_L} \Lambda_\Omega^{(e_L)} \not{X} \mathbf{L}_L \right. \\ & + \frac{2}{3} \overline{\mathbf{u}_R} \Lambda_\xi^{(u_R)} \not{X} \mathbf{u}_R - \frac{1}{3} \overline{\mathbf{d}_R} \Lambda_\xi^{(d_R)} \not{X} \mathbf{d}_R \\ & \left. + \frac{2}{3} \overline{\mathbf{e}_R} \Lambda_\Psi^{(e_R)} \not{X} \mathbf{e}_R \right). \end{aligned} \quad (7)$$

The matrices $\Lambda_\Omega^{(I)}$ and $\Lambda_\Psi^{(I)}$ are defined in (5), where

$$\Omega = \begin{pmatrix} 0 & 0 & 0 \\ 0 & 1 & 0 \\ 0 & 0 & -\frac{5}{8} \end{pmatrix}, \quad \Psi = \begin{pmatrix} 0 & 0 & 0 \\ 0 & 1 & 0 \\ 0 & 0 & -\frac{5}{2} \end{pmatrix}. \quad (8)$$

2.4 Fermion mixing ansatz

The CKM matrix and the PMNS matrix are predicted to be

$$V = V_{u_L}^\dagger V_{d_L}, \quad U = U_{\nu_L}^\dagger V_{e_L}, \quad (9)$$

respectively. For all of the third family hypercharge models that we address here, the matrix element $(V_{d_L})_{23}$ must

be non-zero in order to obtain new physics contributions of the sort required to explain the NCBA's. Moreover, in the Y_3 model we need $(V_{e_L})_{23} \neq 0$ in order to generate a coupling (here left-handed) to muons⁷. These will lead to a BSM contribution to a Lagrangian density term in the weak effective theory proportional to $(\bar{b}\gamma^\mu P_L s)(\bar{\mu}\gamma_\mu P_L \mu)$, where P_L is the left-handed projection operator, which previous fits to the weak effective theory indicate is essential in order to fit the NCBA's [17–23].

In order to investigate the model further phenomenologically, we must assume a particular ansatz for the unitary fermion mixing matrices V_I . Here, for V_{d_L} , we choose the ‘standard parameterisation’ often used for the CKM matrix [74]. This is a parameterisation of a family of unitary 3 by 3 matrices that depends only upon one complex phase and three mixing angles (a more general parameterisation would also depend upon five additional complex phases):

$$\begin{pmatrix} c_{12}c_{13} & s_{12}c_{13} & s_{13}e^{-i\delta} \\ -s_{12}c_{23} - c_{12}s_{23}s_{13}e^{i\delta} & c_{12}c_{23} - s_{12}s_{23}s_{13}e^{i\delta} & s_{23}c_{13} \\ s_{12}s_{23} - c_{12}c_{23}s_{13}e^{i\delta} & -c_{12}s_{23} - s_{12}c_{23}s_{13}e^{i\delta} & c_{23}c_{13} \end{pmatrix}, \quad (10)$$

where $s_{ij} := \sin \theta_{ij}$ and $c_{ij} := \cos \theta_{ij}$, for angles θ_{ij} , $\delta \in \mathbb{R}/(2\pi\mathbb{Z})$. To define our particular ansatz, we choose angles such that $(V_{d_L})_{ij} = V_{ij}$ for all $ij \neq 23$, *i.e.* we insert the current world-averaged measured central values of θ_{ij} and δ [74], *except* for the crucial mixing angle θ_{23} , upon which the NCBA's sensitively depend. Thus, we fix the angles and phase such that $s_{12} = 0.22650$, $s_{13} = 0.00361$ and $\delta = 1.196$ but allow θ_{23} to float as a free parameter in our global fits. Following Refs. [41, 43], we choose simple forms for the other mixing matrices which are likely to evade strict FCNC bounds. Specifically, we choose $V_{d_R} = 1$, $V_{u_R} = 1$ and

$$V_{e_L} = \begin{pmatrix} 1 & 0 & 0 \\ 0 & 0 & 1 \\ 0 & 1 & 0 \end{pmatrix} \quad (11)$$

in the Y_3 model⁸, and $V_{e_L} = 1$ in the DY'_3 model. Finally, V_{u_L} and V_{ν_L} are then fixed by (9) and the measured CKM/PMNS matrix entries. For the remainder of this paper, when referring to the Y_3 model or the DY'_3 model, we shall implicitly refer to the versions given by this mixing ansatz (which, we emphasise, is taken to be the same for all third family hypercharge models aside from the assignment of V_{e_L}).

Next, we turn to calculating the complete set of dimension-6 WCs in the SMEFT that result from integrating the X boson out of the theory.

⁷ The DY_3 model (DY'_3 model) does not require $(V_{e_L})_{23} \neq 0$ to fit the NCBA's, since it already possesses a coupling to μ_L .

⁸ Note that in the Y_3 model, this is equivalent to instead setting $V_{e_L} = 1$ and switching the $U(1)_X$ charges of L_2 and L_3 in Table 2.

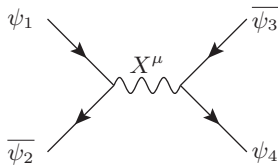


Fig. 1. X -boson mediated process responsible for the effective vertex between 4 fermionic fields $\{\psi_i\}$.

3 SMEFT Coefficients

So far, particle physicists have found scant direct evidence of new physics below the TeV scale. This motivates the study of BSM models whose new degrees of freedom reside at the TeV scale or higher. In such scenarios, it makes sense to consider the Standard Model as an effective field theory realisation of the underlying high energy model. If one wishes to remain agnostic about further details of the high energy theory, this amounts to including all possible operators consistent with the SM gauge symmetries and performing an expansion in powers of the ratio of the electroweak and new physics scales.

The Standard Model Effective Field Theory [75–77] is such a parameterisation of the effects of heavy fields beyond the SM (such as a heavy X boson field of interest to us here) through $d > 4$ operators built out of the SM fields. In this paper we will work with operators up to dimension 6 (*i.e.* we will go to second order in the power expansion). Expanding the SMEFT to this order gives us a very good approximation to all of the observables we consider; the relevant expansion parameter for the EWPOs is $(M_Z/M_X)^2 \ll 1$, and in the case of observables derived from the decay of a meson of mass m , the relevant expansion parameter is $(m/M_X)^2 \ll 1$. By restricting to the $M_X > 1$ TeV region, we ensure that both of these mass ratios are small enough to yield a good approximation.

The SMEFT Lagrangian can be expanded as

$$\mathcal{L}_{\text{SMEFT}} = \mathcal{L}_{\text{SM}} + C_5 O_5 + \sum_{\text{dim } 6} C_i O_i + \dots, \quad (12)$$

where O_5 schematically indicates Weinberg operators with various flavour indices, which result in neutrino masses and may be obtained by adding heavy gauge singlet chiral fermions to play the role of right-handed neutrinos. The sum that is explicitly notated then runs over all mass dimension-6 SMEFT operators, and the ellipsis represents terms which are of mass dimension (in the fields) greater than 6. The WCs C_i have units of $[\text{mass}]^{-2}$. In the following we shall work in the Warsaw basis, which defines a basis in terms of a set of independent baryon-number-conserving operators [78]. By performing the matching between our models and the SMEFT, we shall obtain the set of WCs C_i at the scale M_X , which can then be used to calculate predictions for observables.

To see where these dimension-6 operators come from, let us first consider the origin of four-fermion operators. We may write the fermionic couplings of the underlying theory of the X boson, given in (4) and (7) for the Y_3

model and DY_3' model respectively, as

$$\mathcal{L}^\psi = -J_\psi^\mu X_\mu, \quad (13)$$

where

$$J_\psi^\mu = \sum_{\psi_{i,j}} \kappa_{ij} \bar{\psi}_i \gamma^\mu \psi_j \quad (14)$$

is the fermionic current that the X boson couples to, where the sum runs over all pairs of SM Weyl fermions ψ_i . The couplings κ_{ij} are identified from (4) or (7), depending upon the model. After integrating out the X boson in processes such as the one in Fig. 1, one obtains the following terms in the effective Lagrangian:

$$\mathcal{L}_{\text{SMEFT}} \supset -\frac{J_{\psi_\mu} J_{\psi^\mu}}{2M_X^2}. \quad (15)$$

We match the terms thus obtained with the four-fermion operators in the Warsaw basis [78] in order to identify the 4-fermion SMEFT WCs in that basis.

These 4-fermion operators are not the only SMEFT operators that are produced at dimension-6 by integrating out the X bosons of our models. Due to the tree-level $U(1)_X$ charge of the SM Higgs, there are also various operators in the Higgs sector of the SMEFT, as follows. The (linear) couplings of the X boson to the Higgs, as recorded in (3), can again be written as the coupling of X_μ to a current, *viz.*

$$\mathcal{L}^\phi = -J_{\phi_\mu} X^\mu, \quad (16)$$

where this time

$$J_{\phi_\mu} = i\frac{g_X}{2} \phi^\dagger D_\mu^{\text{SM}} \phi + \text{h.c.} \quad (17)$$

is the bosonic current to which the X boson couples, where $D_\mu^{\text{SM}} = \partial_\mu + i\frac{g}{2}\sigma^a W_\mu^a + i\frac{g'}{2}B_\mu$. Due to the presence of X boson couplings to operators which are bi-linear in both the fermion fields (J_ψ^μ) and the Higgs field (J_ϕ^μ), integrating out the X bosons gives rise to cross-terms

$$\mathcal{L}_{\text{SMEFT}} \supset -\frac{J_{\phi_\mu} J_{\psi^\mu}}{M_X^2}, \quad (18)$$

which encode dimension-6 operators involving two Higgs fields, one SM gauge boson, and a fermion bi-linear current. Diagrammatically, these operators are generated by integrating out the X boson from Feynman diagrams such as that depicted in Fig. 2.

Finally, there are terms that are quadratic in the bosonic current J_ϕ^μ ,

$$\mathcal{L}_{\text{SMEFT}} \supset -\frac{J_{\phi_\mu} J_{\phi^\mu}}{2M_X^2}, \quad (19)$$

which encode dimension-6 operators involving four Higgs fields and two SM covariant derivatives. The corresponding Feynman diagram is given in Fig. 3.

This accounts, schematically, for the complete set of dimension-6 WCs generated by either the Y_3 model or the

DY_3' model⁹. We tabulate all the non-zero WCs generated in this way in Table 4 for the Y_3 model and in Table 5 for the DY_3' model.

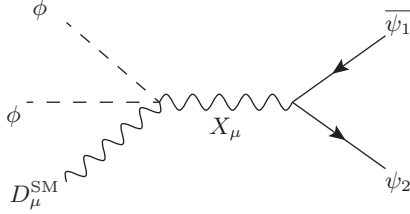


Fig. 2. X -boson mediated process responsible for the effective vertex between two Higgs fields, one SM gauge boson, and a fermion bi-linear operator.

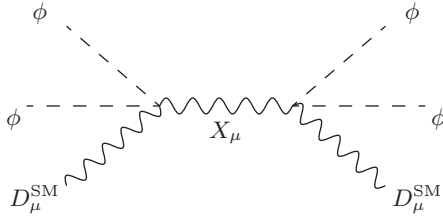


Fig. 3. X -boson mediated process responsible for dimension-6 operators involving four Higgs insertions and either two derivatives or two SM gauge boson insertions.

4 Global Fits

Given the complete sets of dimension-6 WCs (Tables 4 and 5) as inputs at the renormalisation scale M_X ,¹⁰ we use the `smelli-2.2.0` program to calculate hundreds of observables and the resulting likelihoods. The `smelli-2.2.0` program is based upon the observable calculator `flavio-2.2.0` [79], using `Wilson-2.1` [80] for running and matching WCs using the `WCxf` exchange format [81].

In a particular third family hypercharge model, for given values of our three input parameters θ_{23} , g_X , M_X , the WCs in the tables are converted to the non-redundant

⁹ Note that in deriving the WCs we have assumed that the kinetic mixing between the X boson field strength and the hypercharge field strength is negligible at the scale of its derivation, *i.e.* at M_X .

¹⁰ Strictly speaking, the parameters g_X and θ_{23} that we quote are also implicitly evaluated at a renormalisation scale of M_X throughout this paper.

WC	value	WC	value
C_{ll}^{2222}	$-\frac{1}{8}$	$(C_{lq}^{(1)})^{22ij}$	$\frac{1}{12}A_{\xi ij}^{(d_L)}$
$(C_{qq}^{(1)})^{ijkl}$	$A_{\xi ij}^{(d_L)}A_{\xi kl}^{(d_L)}\frac{\delta_{ik}\delta_{jl}-2}{72}$	C_{ee}^{3333}	$-\frac{1}{2}$
C_{uu}^{3333}	$-\frac{2}{9}$	C_{dd}^{3333}	$-\frac{1}{18}$
C_{eu}^{3333}	$\frac{2}{3}$	C_{ed}^{3333}	$-\frac{1}{3}$
$(C_{ud}^{(1)})^{3333}$	$\frac{2}{9}$	C_{le}^{2233}	$-\frac{1}{2}$
C_{lu}^{2233}	$\frac{1}{3}$	C_{ld}^{2233}	$-\frac{1}{6}$
C_{qe}^{ij33}	$\frac{1}{6}A_{\xi ij}^{(d_L)}$	$(C_{qu}^{(1)})^{ij33}$	$-\frac{1}{9}A_{\xi ij}^{(d_L)}$
$(C_{qd}^{(1)})^{ij33}$	$\frac{1}{18}A_{\xi ij}^{(d_L)}$	$(C_{\phi l}^{(1)})^{22}$	$\frac{1}{4}$
$(C_{\phi q}^{(1)})^{ij}$	$-\frac{1}{12}A_{\xi ij}^{(d_L)}$	$C_{\phi e}^{33}$	$\frac{1}{2}$
$C_{\phi u}^{33}$	$-\frac{1}{3}$	$C_{\phi d}^{33}$	$\frac{1}{6}$
$C_{\phi D}$	$-\frac{1}{2}$	$C_{\phi\Box}$	$-\frac{1}{8}$

Table 4. Non-zero dimension-6 SMEFT WCs predicted by the Y_3 model, in units of g_X^2/M_X^2 , in the Warsaw basis [78]. We have highlighted the coefficient (for $i = 2, j = 3$) that is primarily responsible for the NCBA's in bold font.

WC	value	WC	value
C_{ll}^{2222}	$-\frac{25}{72}$	C_{ll}^{2233}	$\frac{10}{9}$
C_{3333}^{3333}	$-\frac{8}{9}$	$(C_{lq}^{(1)})^{22ij}$	$-\frac{5}{36}A_{\xi ij}^{(d_L)}$
$(C_{lq}^{(1)})^{33ij}$	$\frac{2}{9}A_{\xi ij}^{(d_L)}$	$(C_{qq}^{(1)})^{ijkl}$	$A_{\xi ij}^{(d_L)}A_{\xi kl}^{(d_L)}\frac{\delta_{ik}\delta_{jl}-2}{72}$
C_{ee}^{2222}	$-\frac{2}{9}$	C_{ee}^{2233}	$\frac{10}{9}$
C_{ee}^{3333}	$-\frac{25}{18}$	C_{uu}^{3333}	$-\frac{2}{9}$
C_{dd}^{3333}	$-\frac{1}{18}$	C_{eu}^{2233}	$-\frac{4}{9}$
C_{eu}^{3333}	$\frac{10}{9}$	C_{ed}^{2233}	$\frac{2}{9}$
C_{ed}^{3333}	$-\frac{5}{9}$	$(C_{ud}^{(1)})^{3333}$	$\frac{2}{9}$
C_{le}^{2222}	$-\frac{5}{9}$	C_{le}^{2233}	$\frac{25}{18}$
C_{le}^{3333}	$-\frac{20}{9}$	C_{le}^{3322}	$\frac{8}{9}$
C_{lu}^{2233}	$-\frac{5}{9}$	C_{lu}^{3333}	$\frac{8}{9}$
C_{ld}^{2233}	$\frac{5}{18}$	C_{ld}^{3333}	$-\frac{4}{9}$
C_{qe}^{ij22}	$-\frac{1}{9}A_{\xi ij}^{(d_L)}$	C_{qe}^{ij33}	$\frac{5}{18}A_{\xi ij}^{(d_L)}$
$(C_{qu}^{(1)})^{ij33}$	$-\frac{1}{9}A_{\xi ij}^{(d_L)}$	$(C_{qd}^{(1)})^{ij33}$	$\frac{1}{18}A_{\xi ij}^{(d_L)}$
$(C_{\phi l}^{(1)})^{22}$	$-\frac{5}{12}$	$(C_{\phi l}^{(1)})^{33}$	$\frac{2}{3}$
$(C_{\phi q}^{(1)})^{ij}$	$-\frac{1}{12}A_{\xi ij}^{(d_L)}$	$C_{\phi e}^{22}$	$-\frac{1}{3}$
$C_{\phi e}^{33}$	$\frac{5}{6}$	$C_{\phi u}^{33}$	$-\frac{1}{3}$
$C_{\phi d}^{33}$	$\frac{1}{6}$	$C_{\phi D}$	$-\frac{1}{2}$
$C_{\phi\Box}$	$-\frac{1}{8}$		

Table 5. Non-zero dimension-6 SMEFT WCs predicted by the DY_3' model, in units of g_X^2/M_X^2 , in the Warsaw basis [78]. We have highlighted the coefficient that is primarily responsible (for $i = 2, j = 3$) for the NCBA's in bold font. WCs for the original DY_3 model may be obtained by switching the l indices $2 \leftrightarrow 3$ everywhere.

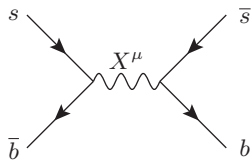


Fig. 4. An X -boson mediated contribution to $B_s - \overline{B}_s$ mixing.

basis [67] assumed by `smelli-2.2.0`¹¹ (a subset of the Warsaw basis). The renormalisation group equations are then solved in order to run the WCs down to the weak scale, at which the EWPOs are calculated. Most of the EWPOs and correlations are taken from Ref. [82] by `smelli-2.2.0`, which neglects the relatively small theoretical uncertainties in EWPOs. The EWPOs have not been averaged over lepton flavour, since lepton flavour non-universality is a key feature of any model of the NCBA, including those built on third family hypercharge which we consider.

We have updated the data used by `flavio-2.2.0` with 2021 LHCb measurements of $BR(B_{d,s} \rightarrow \mu^+ \mu^-)$ taken on 9 fb^{-1} of LHC Run II data [8] by using the two dimensional Gaussian fit to current CMS, ATLAS and LHCb measurements presented in Ref. [83]:

$$\begin{aligned} BR(B_s \rightarrow \mu^+ \mu^-) &= (2.93 \pm 0.35) \times 10^{-9}, \\ BR(B^0 \rightarrow \mu^+ \mu^-) &= (0.56 \pm 0.70) \times 10^{-10}, \end{aligned} \quad (20)$$

with an error correlation of $\rho = -0.27$. The most recent measurement by LHCb in the di-lepton invariant mass squared bin $1.1 < Q^2/\text{GeV}^2 < 6.0$ is

$$R_K = 0.846_{-0.039-0.012}^{+0.042+0.013}, \quad (21)$$

where the first error is statistical and the second systematic [3] (this measurement alone has a 3.1σ tension with the SM prediction of 1.00). We incorporate this new measurement by fitting the log likelihood function presented in Ref. [3] with a quartic polynomial.

The SMEFT weak scale WCs are then matched to the weak effective theory and renormalised down to the scale of bottom mesons using QCD \times QED. Observables relevant to the NCBA are calculated at this scale. `smelli-2.2.0` then organises the calculation of the χ^2 statistic to quantify a distance (squared) between the theoretical prediction and experimental observables in units of the uncertainty. In calculating the χ^2 value, experimental correlations between different observables are parameterised and taken into account. Theoretical uncertainties are modelled as being multi-variate Gaussians; they include the effects of varying nuisance parameters and are approximated to be independent of new physics. Theory uncertainties and experimental uncertainties are then combined in quadrature.

We note that an important constraint on Z' models that explain the NCBA is that from Δm_s (included by

data set	χ^2	n	p -value
quarks	192.3	167	.072
LFU FCNCs	21.0	21	.34
EWPOs	36.0	31	.17
global	249.3	219	.065

Table 6. Goodness of fit for the different data sets we consider for the Y_3 model as calculated by `smelli-2.2.0` for $M_X = 3 \text{ TeV}$. We display the total χ^2 for each data set along with the number of observables n and the data set's p -value. The data set named 'quarks' contains $BR(B_s \rightarrow \phi \mu^+ \mu^-)$, $BR(B_s \rightarrow \mu^+ \mu^-)$, Δm_s and various differential distributions in $B \rightarrow K^{(*)} \mu^+ \mu^-$ decays among others, whereas 'LFU FCNCs' contains $R_{K^{(*)}}$ and some B meson decay branching ratios into di-taus. Our data sets are identical to those defined by `smelli-2.2.0` and we refer the curious reader to its manual [67], where the observables are enumerated. We have updated to R_K and $BR(B_{s,d} \rightarrow \mu^+ \mu^-)$ with the latest LHCb measurements as detailed in §4. Two free parameters of the model were fitted: $\theta_{23} = -0.145$ and $g_X = 0.426$.

`smelli-2.2.0` in the category of 'quarks' observables), deriving from measurements of $B_s - \overline{B}_s$ mixing, because of the tree-level BSM contribution to the process depicted in Fig. 4. The impact of this constraint has significantly varied over the last decade, to a large degree because of numerically rather different lattice or theory inputs used to extract the measurement [84–86]. Here, we are wedded to the calculation and inputs used by `smelli-2.2.0`, allowing some tension in Δm_s to be traded against tension present in the NCBA.

As we shall see, in all the models that we consider the global fit is fairly insensitive to M_X , provided we specify $M_X > 2 \text{ TeV}$ or so in order to be sure to not contravene ATLAS di-muon searches [43, 64, 65]. We will demonstrate this insensitivity to M_X below (see Figs. 9 and 15), but for now we shall pick $M_X = 3 \text{ TeV}$ and scan over the pair ($g_X \times 3 \text{ TeV}/M_X$) and θ_{23} . Since the WCs at M_X all scale like g_X/M_X , the results will approximately hold at different values of M_X provided that g_X is scaled linearly with M_X . The running between M_X and the weak scale breaks this scaling, but such effects derive from loop corrections $\propto (1/16\pi^2) \ln(M_X/M_Z)$ and are thus negligible to a good approximation.

4.1 Y_3 model fit results

The result of fitting θ_{23} and g_X for $M_X = 3 \text{ TeV}$ is shown in Table 6 for the Y_3 model. The 'global' p -value is calculated by assuming a χ^2 distribution with $n - 2$ degrees of freedom, since two parameters were optimised. The fit is encouragingly of a much better quality than the one of the SM. We see that the fits to the EWPOs and NCBA are simultaneously reasonable.

The EWPOs are shown in more detail in Fig. 5, in which we compare some pulls in the SM fit versus the Y_3 model best-fit point. We see that there is some improvement in the prediction of the W -boson mass, which the SM fit predicts is almost 2σ too low (as manifest in

¹¹ `Jupyter` notebooks (from which all data files and plots may be generated) have been stored in the `anc/` subdirectory of the `arXiv` version of this paper.

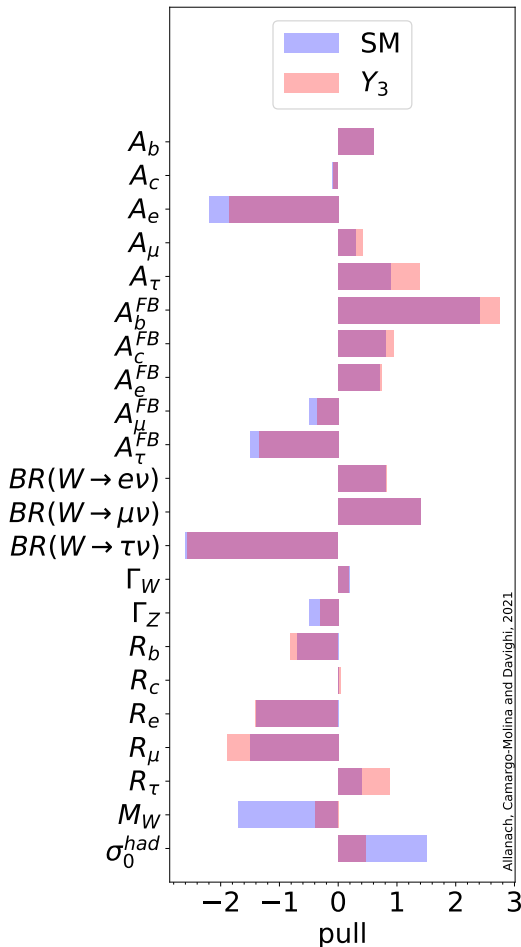


Fig. 5. Pulls in the EWPOs for the Y_3 model $M_X = 3$ TeV best-fit point: $\theta_{23} = -0.145$, $g_X = 0.426$. The pull is defined to be the theory prediction minus the central value of the observation, divided by the combined theoretical and experimental uncertainty, neglecting any correlations with other observables.

the ρ -parameter being measured to be slightly larger than one [74], for M_Z taken to be fixed to its SM value). The easing of this tension in M_W is due precisely to the $Z - Z'$ mixing in the (D) Y_3 models. The non-zero value of the SMEFT coefficient $C_{\phi D}$ breaks custodial symmetry, resulting in a shift of the ρ -parameter away from its tree-level SM value of one, to [66]

$$(\rho_0)_{Y_3} = 1 - C_{\phi D} v^2 / 2 = 1 + v^2 g_X^2 / (4m_X^2). \quad (22)$$

where v is the SM Higgs VEV. Rather than being dangerous, as might reasonably have been guessed, it turns out that this BSM contribution to ρ_0 is in large part responsible for the Y_3 model fitting the EWPOs approximately as well as the SM does.

We also see that σ_0^{had} , the e^+e^- scattering cross-section to hadrons at a centre-of-mass energy of M_Z , is better fit by the Y_3 model than the SM. Although the other EWPOs have some small deviations from their SM fits, the overall picture is that the Y_3 model best-fit point has an electroweak fit similar to that of the SM.

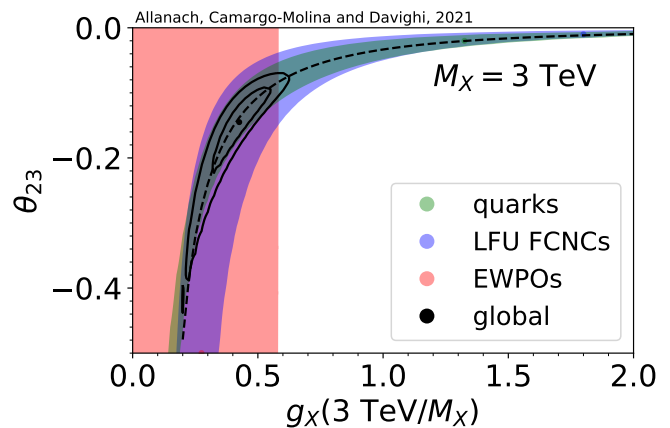


Fig. 6. Two parameter fit to the Y_3 model for $M_X = 3$ TeV. Shaded regions are those preferred by the data set in the legend at the 95% confidence level (CL). The global fit is shown by the solid curves, where the inner (outer) curves show the 70%(95%) CL regions, respectively. The set named ‘quarks’ contains $BR(B_s \rightarrow \phi \mu^+ \mu^-)$, $BR(B_s \rightarrow \mu^+ \mu^-)$, Δm_s and various differential distributions in $B \rightarrow K^{(*)} \mu^+ \mu^-$ decays among others, whereas ‘LFU FCNCs’ contains $R_{K^{(*)}}$ and some B meson decay branching ratios into di-taus. Our sets are identical to those defined by `smelli-2.2.0` and we refer the curious reader to its manual [67], where the observables are enumerated. We have updated R_K and $BR(B_{s,d} \rightarrow \mu^+ \mu^-)$ with the latest LHCb measurements as detailed in §4. The black dot marks the locus of the best-fit point.

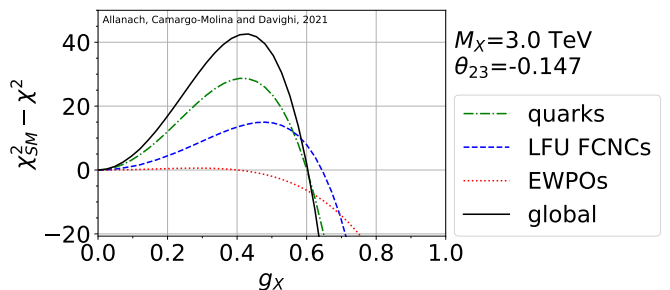


Fig. 7. Y_3 model $\Delta\chi^2$ contributions in the vicinity of the best-fit point as a function of g_X .

In order to see which areas of parameter space are favoured by the different sets of constraints, we provide Fig. 6. The figure shows that the EWPOs and different sets of NCBA data all overlap at the 95% CL. The best-fit point has a total χ^2 of 43 less than that of the SM and is marked by a black dot. The separate data set contributions to χ^2 at this point are listed in Table 6. In order to calculate 70% (95%) CL bounds in the 2-dimensional parameter plane, we draw contours of χ^2 equal to the best-fit value plus 2.41 (5.99) respectively, using the combined χ^2 incorporating all the datasets.

We further study the different χ^2 contributions for the Y_3 model in the vicinity of the best-fit point in Figs. 7-

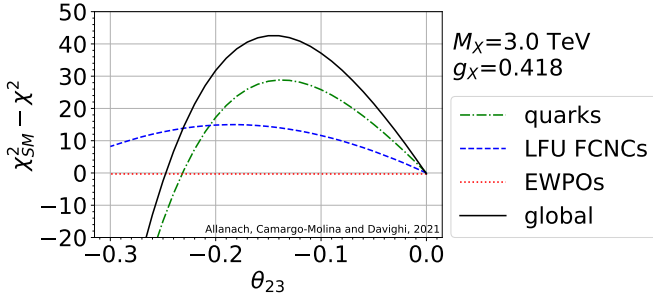


Fig. 8. Y_3 model $\Delta\chi^2$ contributions in the vicinity of the best-fit point as a function of θ_{23} .

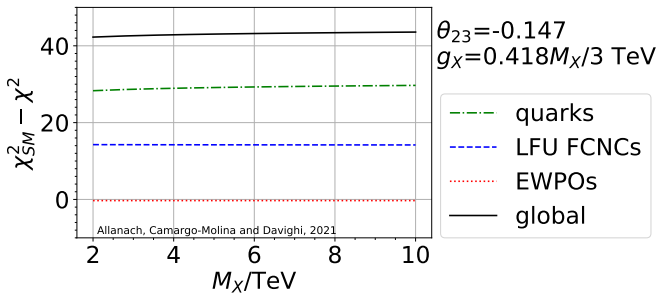


Fig. 9. Y_3 model $\Delta\chi^2$ contributions in the vicinity of the best-fit point as a function of M_X , where g_X has been scaled linearly.

9. From Fig. 7, we see that large couplings $g_X > 0.6$ are disfavoured by EWPOs as well as the NCBA. From Fig. 8 we see that the EWPOs are insensitive to the value of θ_{23} in the vicinity of the best-fit point but the NCBA are not. At large $-\theta_{23}$ the Y_3 model suffers due to a bad fit to the $B_s - \bar{B}_s$ mixing observable Δm_s . In Fig. 9, we demonstrate the approximate insensitivity of χ^2 near the best-fit point to M_X , provided that g_X is scaled linearly with it.

Finally, we display some individual observables of interest in Fig. 10 at the Y_3 model best-fit point. While some of the prominent NCBA measurements (for example R_K in the bin of $m_{\mu\mu}^2$ between 1.1 GeV² and 6 GeV²) fit considerably better than the SM, we see that this is partly compensated by a worse fit in Δm_s , as is the case for many Z' models for the NCBA. The P_5' observable (derived in terms of angular distributions of $B^0 \rightarrow K^* \mu^+ \mu^-$ decays [87, 88]) shows no significant change from the SM prediction in the bin that deviates the most significantly from experiment: $m_{\mu\mu}^2 \in (4, 6)$ GeV², as measured by LHCb [12] and ATLAS [13]. The fit to $BR(\Lambda_b \rightarrow \Lambda \mu^+ \mu^-)$ is slightly worse than that of the SM in one particular bin, as shown in the figure. Some other flavour observables in the flavour sector, notably various bins of $BR(B \rightarrow K^{(*)} \mu^+ \mu^-)$, show some small differences in pulls between the SM and the Y_3 model. Whilst there are many of these and in aggregate they make a difference to the overall χ^2 , there is no small set of observables that pro-

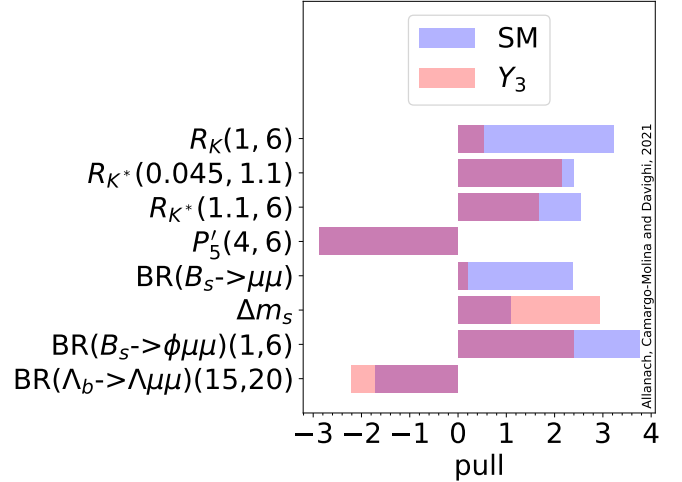


Fig. 10. Pulls of interest for the Y_3 model $M_X = 3$ TeV best-fit point: $\theta_{23} = -0.145$, $g_X = 0.426$. The pull is defined to be the theory prediction minus the central value of the observation, divided by the combined theoretical and experimental uncertainty, neglecting any correlations with other observables. Numbers in brackets after the observable name refer to minimum and maximum values of $m_{\mu\mu}^2$ of the bin in GeV², respectively (many other bins and observables are also used to compute the global likelihood).

data set	χ^2	n	p -value
quarks	196.6	167	.047
LFU FCNCs	20.2	21	.39
EWPOs	37.2	31	.14
global	253.9	219	.044

Table 7. Goodness of fit for the different data sets we consider for the DY_3' model, as calculated by `smelli-2.2.0` for $M_X = 3$ TeV. We display the total χ^2 for each data set along with the number of observables n and the data set's p -value. The set named 'quarks' contains $BR(B_s \rightarrow \phi \mu^+ \mu^-)$, $BR(B_s \rightarrow \mu^+ \mu^-)$, Δm_s and various differential distributions in $B \rightarrow K^{(*)} \mu^+ \mu^-$ decays among others, whereas 'LFU FCNCs' contains $R_{K^{(*)}}$ and some B meson decay branching ratios into di-taus. Our sets are identical to those defined by `smelli-2.2.0` and we refer the curious reader to its manual [67], where the observables are enumerated. We have updated R_K and $BR(B_{s,d} \rightarrow \mu^+ \mu^-)$ with the latest LHCb measurements as detailed in §4. Two free parameters of the model were fitted: $\theta_{23} = -0.181$ and $g_X = 0.253$.

vide the driving force and so we neglect to show them¹². We shall now turn to the DY_3' model fit results, where these comments about flavour observables also apply.

4.2 DY_3' model fit results

We summarise the quality of the fit for the DY_3' model at the best-fit point, for $M_X = 3$ TeV, in Table 7. We

¹² The interested reader can find values for all observables and pulls in the `Jupyter` notebook in the ancillary information associated with the `arXiv` version of this paper.

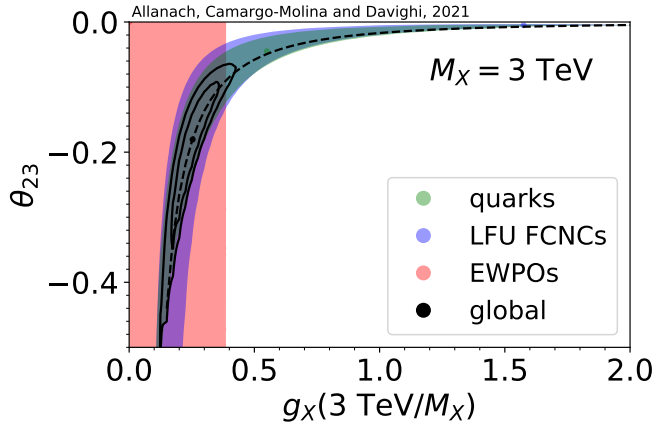


Fig. 11. Two parameter fit to the DY'_3 model for $M_X = 3$ TeV. Shaded regions are those preferred by the data set in the legend at the 95% confidence level (CL). The global fit is shown by the solid curves, where the inner (outer) curves show the 70% (95%) CL regions, respectively. The set named ‘quarks’ contains $BR(B_s \rightarrow \phi\mu^+\mu^-)$, $BR(B_s \rightarrow \mu^+\mu^-)$, Δm_s and various differential distributions in $B \rightarrow K^{(*)}\mu^+\mu^-$ decays among others, whereas ‘LFU FCNCs’ contains $R_{K^{(*)}}$ and some B meson decay branching ratios into di-taus. Our sets are identical to those defined by `smelli-2.2.0` and we refer the curious reader to its manual [67], where the observables are enumerated. We have updated R_K and $BR(B_{s,d} \rightarrow \mu^+\mu^-)$ with the latest LHCb measurements as detailed in §4. The black dot marks the locus of the best-fit point.

see a much improved fit as compared to the SM (by a $\Delta\chi^2 = 39$) and a similar (but slightly worse) quality of fit compared to the Y_3 model, as a comparison with Table 6 shows.

The constraints upon the parameters θ_{23} and g_X are shown in Fig. 11. Although the figure is for $M_X = 3$ TeV, the picture remains approximately the same for $2 < M_X/\text{TeV} < 10$. We see that, as is the case for the Y_3 model, there is a region of overlap of the 95% CL regions of all of the constraints.

The pulls in the EWPOs for the best-fit point of the DY'_3 model are shown in Fig. 12. Like the Y_3 model above, we see a fit comparable in quality to that of the SM. Again, the DY'_3 model predicts M_W to be a little higher than in the SM, agreeing slightly better with the experimental measurement.

The behaviour of the fit in various directions in parameter space around the best-fit point is shown in Figs. 13-15. Qualitatively, this behaviour is similar to that of the Y_3 model: the EWPOs and NCBAs imply that g_X should not become too large. The mixing observable Δm_s prevents $-\theta_{23}$ from becoming too large, and the fits are insensitive to M_X varied between 2 TeV and 10 TeV so long as g_X is scaled linearly with M_X .

Fig. 16 shows various pulls of interest at the best-fit point of the DY'_3 model. Better fits (than the SM) to sev-

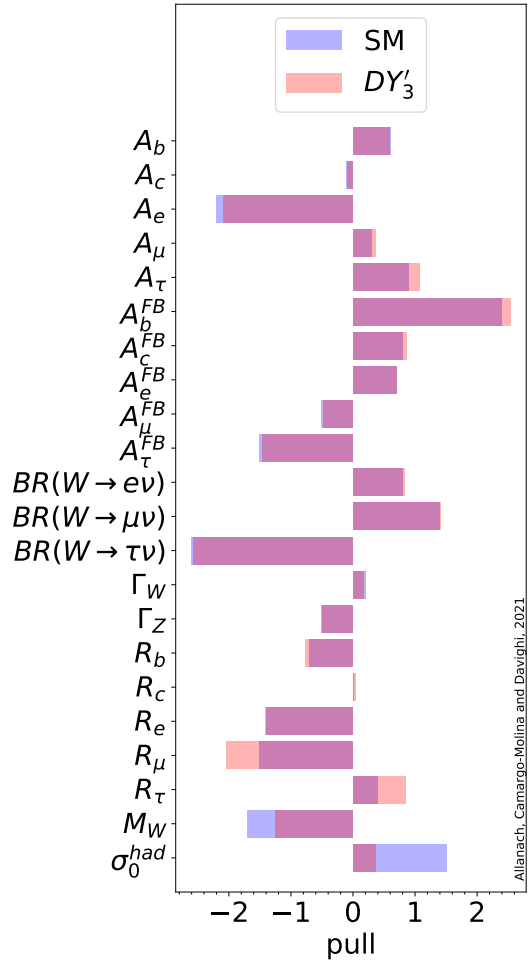


Fig. 12. Pulls in the EWPOs for the $M_X = 3$ TeV DY'_3 model best-fit point: $g_X = 0.253$, $\theta_{23} = -0.181$. The pull is defined to be the theory prediction minus the central value of the observation, divided by the combined theoretical and experimental uncertainty, neglecting any correlations with other observables.

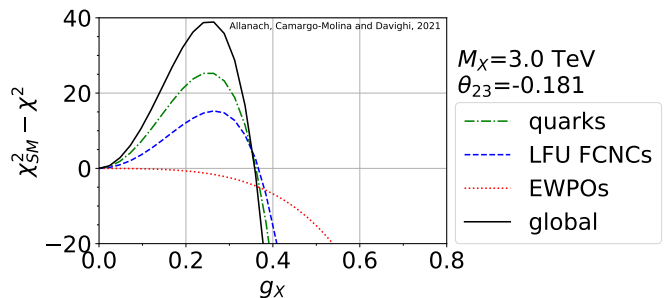


Fig. 13. $\Delta\chi^2$ contributions in the vicinity of the DY'_3 model best-fit point as a function of g_X .

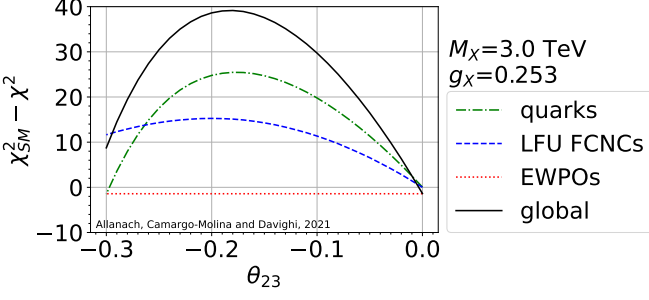


Fig. 14. $\Delta\chi^2$ contributions in the vicinity of the DY_3' model best-fit point as a function of θ_{23} .

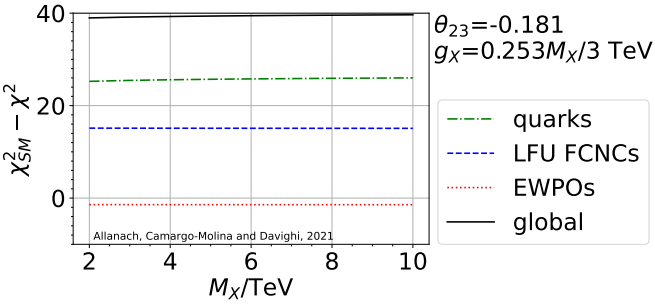


Fig. 15. $\Delta\chi^2$ contributions in the vicinity of the DY_3' model best-fit point as a function of M_X , where g_X has been scaled linearly.

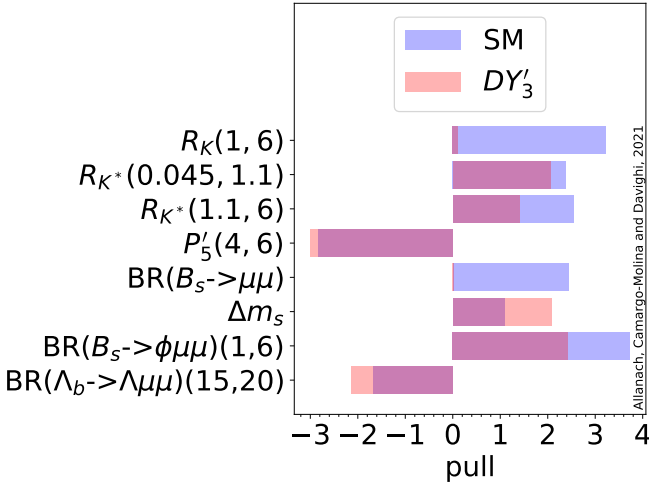


Fig. 16. Pulls of interest for the $M_X = 3$ TeV DY_3' model best-fit point: $g_X = 0.253$, $\theta_{23} = -0.181$. The pull is defined to be the theory prediction minus the central value of the observation, divided by the combined theoretical and experimental uncertainty, neglecting any correlations with other observables. Numbers in brackets after the observable name refer to minimum and maximum values of $m_{\mu\mu}^2$ in GeV^2 , respectively (many other bins and observables are also used to compute the global likelihood).

data set	χ^2	n	p -value
quarks	204.7	167	.019
LFU FCNCs	20.7	21	.35
EWPOs	35.0	31	.2
global	260.5	219	.023

Table 8. Goodness of fit for the different data sets we consider for the original DY_3 model, as calculated by `smelli-2.2.0` for $M_X = 3$ TeV. We display the total χ^2 for each data set along with the number of observables n and the data set's p -value. The set named ‘quarks’ contains $BR(B_s \rightarrow \phi\mu^+\mu^-)$, $BR(B_s \rightarrow \mu^+\mu^-)$, Δm_s and various differential distributions in $B \rightarrow K^{(*)}\mu^+\mu^-$ decays among others, whereas ‘LFU FCNCs’ contains $R_{K^{(*)}}$ and some B meson decay branching ratios into di-taus. Our sets are identical to those defined by `smelli-2.2.0` and we refer the curious reader to its manual [67], where the observables are enumerated. We have updated R_K and $BR(B_{s,d} \rightarrow \mu^+\mu^-)$ with the latest LHCb measurements as detailed in §4. Two free parameters of the model were fitted: $\theta_{23} = 0.122$ and $g_X = 0.428$.

eral NBCA observables are partially counteracted by a worse fit to the Δm_s observable.

4.3 Original DY_3 model fit results

We display the overall fit quality of the original DY_3 model in Table 8. By comparison with Tables 1 and 6 we see that although its predictions still fit the data significantly better than the SM ($\Delta\chi^2$ is 32), the original DY_3 model does not achieve as good fits as the other models. For the sake of brevity, we have refrained from including plots for it¹³. Instead, it is more enlightening to understand the reason behind this slightly worse fit, which is roughly as follows. The coupling of the X boson to muons in the original DY_3 model is close to vector-like, *viz.* $\mathcal{L} = g_X/6(\bar{\mu}\not{X}(5P_L + 4P_R))\mu + \dots$ (where P_L, P_R are left-handed and right-handed projection operators, respectively), which is slightly less preferred by the `smelli-2.2.0` fits than an X boson coupled more strongly to left-handed muons [67]. This preference is in large part due to the experimentally measured value of $BR(B_s \rightarrow \mu^+\mu^-)$, which is somewhat lower than the SM prediction [4–7], and is sensitive only to the axial component of the coupling to muons. Compared to the Y_3 model and the DY_3' model, the fit to $BR(B_s \rightarrow \mu^+\mu^-)$ is worse when the DY_3 model fits other observables well. The p -value is significantly lower than the canonical lower bound of 0.05, indicating a somewhat poor fit.

4.4 The $\theta_{23} = 0$ limit of our models

The NBCAs can receive sizeable contributions even when the tree-level coupling of the X boson to $\bar{b}s$ vanishes. For example, non-zero and $\mathcal{O}(1)$ TeV^2 values for C_{lu}^{2233} (as

¹³ These may be found within a `Jupyter` notebook in the `anc` sub-directory of the `arXiv` submission of this paper.

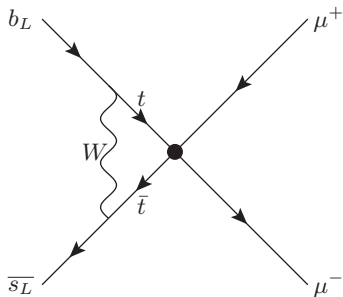


Fig. 17. Example of the W -loop process dominating the SMEFT contribution to the NCBA in the $\theta_{23} = 0$ case. The filled disc marks the location of the BSM operator.

well as non-zero C_{eu}^{2233} in the case of the DY_3 model and the DY_3' model) can give a reasonable fit to the NCBA data [89] via a W -boson loop as in Fig. 17¹⁴ Such a scenario would require that V_{ts} originates from mixing entirely within the up-quark sector. This qualitatively different quark mixing ansatz therefore provides a motivation to consider the $\theta_{23} = 0$ scenario separately. In the $\theta_{23} = 0$ limit, we have that $A_{\xi 23}^{(d_L)}$ is proportional to $s_{13} \ll 1$ meaning that we also predict a negligible $(C_{lq}^{(1)})^{2223}$ at M_X . Meanwhile, C_{lu}^{2233} in the Y_3 model (as well as C_{eu}^{2233} for the DY_3' model and the DY_3 model) remains the same as in the $\theta_{23} \neq 0$ case shown in Tables 4 and 5. We note that contributions to the NCBA arising from W loops such as the one in Fig. 17 are nevertheless always included (through renormalisation group running) by `smelli-2.2.0`, even for $\theta_{23} \neq 0$.

While it is true that much of the tension with the NCBA can be ameliorated by such W loop contributions, we find from our global fits that the corresponding values for g_X^2/M_X^2 are far too large to simultaneously give a good fit to the EWPOs in this $\theta_{23} = 0$ limit. As our results with a floating θ_{23} suggest (see e.g. Fig. 6 along $\theta_{23} = 0$), as far as the EWPOs go, SM-like scenarios are strongly preferred, since EWPOs quickly exclude any region that might resolve the tension with NCBA. This is even more so than for the simplified model studied in [89], where already a significant tension with $Z \rightarrow \mu\mu$ was pointed out. In our case, besides several stringent bounds from other observables measured at the Z^0 -pole for $g_X \approx 1$ and $M_X \approx O(3)$ TeV (which predicts C_{lq}^{2223} just large enough to give a slightly better fit to R_K and R_{K^*} than the SM) the predicted W -boson mass is more than 5σ away from its measured value. This stands in stark contrast with the overall better-than-SM fit we find for M_W when $\theta_{23} \neq 0$.

¹⁴ The connection between the EWPOs and minimal flavour-violating one-loop induced NCBA has recently been addressed in Ref. [90], encoding the inputs in the SMEFT framework. Third family hypercharge models are in a sense orthogonal to this analysis, since they favour particular directions in *non-minimal* flavour violating SMEFT operator space generated already at the *tree-level*. The possibility of accommodating the NCBA through such loop contributions was first pointed out in Ref. [91] with a more general study for $b \rightarrow sll$ transitions presented in Ref. [92].

5 Discussion

Previous explorations of the parameter spaces of third family hypercharge models [41, 43] capable of explaining the neutral current B -anomalies showed the 95% confidence level exclusion regions from various important constraints, but these analyses did not include electroweak precision observables. Collectively, the electroweak precision observables were potentially a model-killing constraint because, through the $Z^0 - Z'$ mixing predicted in the models, the prediction of M_W in terms of M_Z is significantly altered from the SM prediction. This was noticed in Ref. [66], where rough estimates of the absolute sizes of deviations were made. However, the severity of the constraint on the original Third Family Hypercharge (Y_3) Model parameter space was found to depend greatly upon which estimate¹⁵ of the constraint was used. In the present paper, we use the `smelli-2.2.0` [67] computer program to robustly and accurately predict the electroweak precision observables and provide a comparison with empirical measurements. We have thence carried out *global fits* of third family hypercharge models to data pertinent to the neutral current B -anomalies as well as the electroweak precision observables. This is more sophisticated than the previous efforts because it allows tensions between 217 different observables to be traded off against one another in a statistically sound way. In fact, at the best-fit points of the third family hypercharge models, M_W fits *better* than in the SM, whose prediction is some 2σ too low.

One ingredient of our fits was the assumption of a fermion mixing ansatz. The precise details of fermion mixing are expected to be fixed in third family hypercharge models by a more complete ultra-violet model. This could lead to suppressed non-renormalisable operators in the third family hypercharge model effective field theory, for example which, when the flavon acquires its VEV, lead to small mixing effects. Such detailed model building seems premature in the absence of additional information coming from the direct observation of a flavour-violating Z' , or indeed independent precise confirmation of NCBA from the Belle II [93] experiment. Reining in any urge to delve into the underlying model building, we prefer simply to assume a non-trivial structure in the fermion mixing matrix which changes the observables we consider most: those involving the left-handed down quarks. Since the neutral current B -anomalies are most sensitive to the mixing angle between left-handed bottom and strange quarks, we have allowed this angle to float. But the other mixing angles and complex phase in the matrix have been set to some (roughly mandated but ultimately arbitrary) values equal to those in the CKM matrix. We have checked that changing these arbitrary values somewhat (*e.g.* setting them to zero) does not change the fit qualitatively: a change in χ^2 of up to 2 units was observed. It is clear that a more thorough investigation of such variations may be

¹⁵ In more detail, the strength of the constraint was strongly dependent on how many of the oblique parameters S , T , and U were allowed to simultaneously float.

model	χ^2	p -value
SM	292.2	.00068
Y_3	249.3	.065
DY_3	260.5	.023
DY_3'	253.9	.044

Table 9. Comparison of p -values resulting from our global fits of the SM and various third family hypercharge models (with $M_{Z'} = 3$ TeV) to a combination of 219 neutral current B -anomaly and electroweak data.

come interesting in the future, particularly if the NCBA's strengthen because of new measurements.

We summarise the punch line of the global fits in Table 9. We see that, while the SM suffers from a poor fit to the combined data set, the various third family hypercharge models fare considerably better. The model with the best fit is the original Third Family Hypercharge Model (Y_3). We have presented the constraints upon the parameter spaces of the Y_3 model and the DY_3' model in detail in §4. The qualitative behaviour of the Y_3 model and the DY_3' model in the global fit is similar, although the regions of preferred parameters are different.

It is well known that Δm_s provides a strong constraint on models which fit the NCBA's and ours are no exception: in fact, we see in Figs 10,16 that this variable has a pull of 2.7σ (2.1σ) in the Y_3 model (DY_3' model), whereas the SM pull is only 1.1σ , according to the `smelli-2.2.0` calculation. The dominant beyond the SM contribution to Δm_s from our models is proportional to the Z' coupling to $\bar{s}b$ quarks squared, i.e. $[g_X(A_\xi^{(dL)})_{23}/6]^2$. The coupling $(A_\xi^{(dL)})_{23}$ is adjustable because θ_{23} is allowed to vary over the fit, and Δm_s provides an *upper bound* upon $|g_X(A_\xi^{(dL)})_{23}|$. On the other hand, in order to produce a large enough effect in the lepton flavour universality violating observables to fit data, the *product* of the Z' couplings to $\bar{s}b$ quarks and to $\mu^+\mu^-$ must be at least a certain size. Thus, models where the Z' couples more strongly to muons because their $U(1)_X$ charges are larger fare better when fitting the combination of the LFU FCNCs and Δm_s . The Z' coupling to muons is $1/2$ for the Y_3 model and $2/3$ for the DY_3' model, favouring the DY_3' model in this regard.

Despite the somewhat worse fit to Δm_s for the Y_3 model as compared to the DY_3' model, Table 9 shows that, overall, the Y_3 model is a better fit. Looking at the flavour observables in detail, it is hard to divine a single cause for this: it appears to be the accumulated effect of many flavour observables in tandem. The difference in χ^2 between the Y_3 model and the DY_3' model of 4.4 is not large and might merely be the result of statistical fluctuations in the 219 data; indeed 1.2 of this comes from the difference of quality of fit to the EWPOs.

All of the usual caveats levelled at interpreting p -values apply. In particular, p -values change depending upon exactly which observables are included or excluded. We have stuck to pre-defined sets of observables in `smelli-2.2.0` in an attempt to reduce bias. However,

we note that there are other data that are in tension with SM predictions which we have not included, namely the anomalous magnetic moment of the muon $(g-2)_\mu$ and charged current B -anomalies. If we were to include these observables, the p -values of all models in Table 9 would lower. Since third family hypercharge models give the *same* prediction for these observables as the SM, each model would receive the same χ^2 increase as well as the increase in the number of fitted data. However, since our models have essentially nothing to add to these observables compared with the SM, we feel justified in leaving them out from the beginning. We could have excluded some of the observables that `smelli-2.2.0` includes in our data sets (obvious choices include those that do not involve bottom quarks, e.g. ϵ_K) further changing our calculation of the p -values of the various models.

As noted above, as far as the third family hypercharge models currently stand, the Z' contribution to $(g-2)_\mu$ is small [28]. In order to explain an inferred beyond the SM contribution to $(g-2)_\mu$ compatible with current measurements $\Delta(g-2)_\mu/2 \approx 28 \pm 8 \times 10^{-10}$, one may simply add a heavy (TeV-scale) vector-like lepton representation that couples to the muon and the Z' at one vertex. In that case, a one-loop diagram with the heavy leptons and Z' running in the loop is sufficient and is simultaneously compatible with the neutral current B -anomalies and measurements of $(g-2)_\mu$ [28].

Independent corroboration from other experiments and future B -anomaly measurements are eagerly awaited and, depending upon them, a re-visiting of global fits to flavour and electroweak data may well become desirable. We also note that, since electroweak precision observables play a key rôle in our fits, an increase in precision upon them resulting from LHC or future e^+e^- collider data, could also prove to be of great utility in testing third family hypercharge models indirectly. Direct production of the predicted Z' [43, 65] (and a measurement of its couplings) would, along with an observation of *flavonstrahlung* [40], ultimately provide a ‘smoking gun’ signal.

Acknowledgements

This work has been partially supported by STFC Consolidated HEP grants ST/P000681/1 and ST/T000694/1. JECM is supported by the Carl Trygger foundation (grant no. CTS 17:139). We are indebted to M McCullough for raising the question of the electroweak precision observables in the Y_3 model. We thank other members of the Cambridge Pheno Working Group for discussions and D Straub and P Stangl for helpful communications about the nuisance parameters in `smelli-2.2.0`.

References

1. R. Aaij, et al., JHEP **08**, 055 (2017). DOI 10.1007/JHEP08(2017)055
2. R. Aaij, et al., Phys. Rev. Lett. **122**(19), 191801 (2019). DOI 10.1103/PhysRevLett.122.191801

3. R. Aaij, et al., (2021)
4. M. Aaboud, et al., JHEP **04**, 098 (2019). DOI 10.1007/JHEP04(2019)098
5. S. Chatrchyan, et al., Phys. Rev. Lett. **111**, 101804 (2013). DOI 10.1103/PhysRevLett.111.101804
6. V. Khachatryan, et al., Nature **522**, 68 (2015). DOI 10.1038/nature14474
7. R. Aaij, et al., Phys. Rev. Lett. **118**(19), 191801 (2017). DOI 10.1103/PhysRevLett.118.191801
8. K. Petridis, M. Santimaria. New results on theoretically clean observables in rare b-meson decays from lhcb (2021). URL <https://indico.cern.ch/event/976688/>. LHC seminar
9. R. Aaij, et al., JHEP **09**, 179 (2015). DOI 10.1007/JHEP09(2015)179
10. CDF collaboration, CDF-NOTE-10894 (2012)
11. R. Aaij, et al., Phys. Rev. Lett. **111**, 191801 (2013). DOI 10.1103/PhysRevLett.111.191801
12. R. Aaij, et al., JHEP **02**, 104 (2016). DOI 10.1007/JHEP02(2016)104
13. M. Aaboud, et al., JHEP **10**, 047 (2018). DOI 10.1007/JHEP10(2018)047
14. A.M. Sirunyan, et al., Phys. Lett. B **781**, 517 (2018). DOI 10.1016/j.physletb.2018.04.030
15. V. Khachatryan, et al., Phys. Lett. B **753**, 424 (2016). DOI 10.1016/j.physletb.2015.12.020
16. C. Bobeth, M. Chrzaszcz, D. van Dyk, J. Virto, Eur. Phys. J. C **78**(6), 451 (2018). DOI 10.1140/epjc/s10052-018-5918-6
17. M. Algueró, B. Capdevila, A. Crivellin, S. Descotes-Genon, P. Masjuan, J. Matias, M. Novoa Brunet, J. Virto, Eur. Phys. J. C **79**(8), 714 (2019). DOI 10.1140/epjc/s10052-019-7216-3. [Addendum: Eur.Phys.J.C 80, 511 (2020)]
18. A.K. Alok, A. Dighe, S. Gangal, D. Kumar, JHEP **06**, 089 (2019). DOI 10.1007/JHEP06(2019)089
19. M. Ciuchini, A.M. Coutinho, M. Fedele, E. Franco, A. Paul, L. Silvestrini, M. Valli, Eur. Phys. J. C **79**(8), 719 (2019). DOI 10.1140/epjc/s10052-019-7210-9
20. J. Aebischer, W. Altmannshofer, D. Guadagnoli, M. Reboud, P. Stangl, D.M. Straub, Eur. Phys. J. C **80**(3), 252 (2020). DOI 10.1140/epjc/s10052-020-7817-x
21. A. Datta, J. Kumar, D. London, Phys. Lett. B **797**, 134858 (2019). DOI 10.1016/j.physletb.2019.134858
22. K. Kowalska, D. Kumar, E.M. Sessolo, Eur. Phys. J. C **79**(10), 840 (2019). DOI 10.1140/epjc/s10052-019-7330-2
23. A. Arbey, T. Hurth, F. Mahmoudi, D.M. Santos, S. Neshatpour, Phys. Rev. D **100**(1), 015045 (2019). DOI 10.1103/PhysRevD.100.015045
24. R. Gauld, F. Goertz, U. Haisch, Phys. Rev. D **89**, 015005 (2014). DOI 10.1103/PhysRevD.89.015005
25. A.J. Buras, F. De Fazio, J. Girrbach, JHEP **02**, 112 (2014). DOI 10.1007/JHEP02(2014)112
26. A.J. Buras, J. Girrbach, JHEP **12**, 009 (2013). DOI 10.1007/JHEP12(2013)009
27. A.J. Buras, F. De Fazio, J. Girrbach-Noe, JHEP **08**, 039 (2014). DOI 10.1007/JHEP08(2014)039
28. B. Allanach, F.S. Queiroz, A. Strumia, S. Sun, Phys. Rev. D **93**(5), 055045 (2016). DOI 10.1103/PhysRevD.93.055045. [Erratum: Phys.Rev.D 95, 119902 (2017)]
29. J. Ellis, M. Fairbairn, P. Tunney, Eur. Phys. J. C **78**(3), 238 (2018). DOI 10.1140/epjc/s10052-018-5725-0
30. B.C. Allanach, J. Davighi, S. Melville, JHEP **02**, 082 (2019). DOI 10.1007/JHEP02(2019)082. [Erratum: JHEP 08, 064 (2019)]
31. B.C. Allanach, B. Gripaios, J. Tooby-Smith, Phys. Rev. Lett. **125**(16), 161601 (2020). DOI 10.1103/PhysRevLett.125.161601
32. W. Altmannshofer, S. Gori, M. Pospelov, I. Yavin, Phys. Rev. D **89**, 095033 (2014). DOI 10.1103/PhysRevD.89.095033
33. A. Crivellin, G. D'Ambrosio, J. Heeck, Phys. Rev. Lett. **114**, 151801 (2015). DOI 10.1103/PhysRevLett.114.151801
34. A. Crivellin, G. D'Ambrosio, J. Heeck, Phys. Rev. D **91**(7), 075006 (2015). DOI 10.1103/PhysRevD.91.075006
35. A. Crivellin, L. Hofer, J. Matias, U. Nierste, S. Pokorski, J. Rosiek, Phys. Rev. D **92**(5), 054013 (2015). DOI 10.1103/PhysRevD.92.054013
36. W. Altmannshofer, I. Yavin, Phys. Rev. D **92**(7), 075022 (2015). DOI 10.1103/PhysRevD.92.075022
37. J. Davighi, M. Kirk, M. Nardecchia, JHEP **12**, 111 (2020). DOI 10.1007/JHEP12(2020)111
38. R. Alonso, P. Cox, C. Han, T.T. Yanagida, Phys. Lett. B **774**, 643 (2017). DOI 10.1016/j.physletb.2017.10.027
39. C. Bonilla, T. Modak, R. Srivastava, J.W.F. Valle, Phys. Rev. D **98**(9), 095002 (2018). DOI 10.1103/PhysRevD.98.095002
40. B.C. Allanach, Eur. Phys. J. C **81**(1), 56 (2021). DOI 10.1140/epjc/s10052-021-08855-w
41. B.C. Allanach, J. Davighi, JHEP **12**, 075 (2018). DOI 10.1007/JHEP12(2018)075
42. J. Davighi, in *54th Rencontres de Moriond on QCD and High Energy Interactions* (ARISF, 2019)
43. B.C. Allanach, J. Davighi, Eur. Phys. J. C **79**(11), 908 (2019). DOI 10.1140/epjc/s10052-019-7414-z
44. D. Aristizabal Sierra, F. Staub, A. Vicente, Phys. Rev. D **92**(1), 015001 (2015). DOI 10.1103/PhysRevD.92.015001
45. A. Celis, J. Fuentes-Martin, M. Jung, H. Serodio, Phys. Rev. D **92**(1), 015007 (2015). DOI 10.1103/PhysRevD.92.015007
46. A. Greljo, G. Isidori, D. Marzocca, JHEP **07**, 142 (2015). DOI 10.1007/JHEP07(2015)142
47. A. Falkowski, M. Nardecchia, R. Ziegler, JHEP **11**, 173 (2015). DOI 10.1007/JHEP11(2015)173
48. C.W. Chiang, X.G. He, G. Valencia, Phys. Rev. D **93**(7), 074003 (2016). DOI 10.1103/PhysRevD.93.074003
49. S.M. Boucenna, A. Celis, J. Fuentes-Martin, A. Vicente, J. Virto, Phys. Lett. B **760**, 214 (2016). DOI 10.1016/j.physletb.2016.06.067
50. S.M. Boucenna, A. Celis, J. Fuentes-Martin, A. Vicente, J. Virto, JHEP **12**, 059 (2016). DOI 10.1007/JHEP12(2016)059
51. P. Ko, Y. Omura, Y. Shigekami, C. Yu, Phys. Rev. D **95**(11), 115040 (2017). DOI 10.1103/PhysRevD.95.115040
52. R. Alonso, P. Cox, C. Han, T.T. Yanagida, Phys. Rev. D **96**(7), 071701 (2017). DOI 10.1103/PhysRevD.96.071701
53. Y. Tang, Y.L. Wu, Chin. Phys. C **42**(3), 033104 (2018). DOI 10.1088/1674-1137/42/3/033104. [Erratum: Chin.Phys.C 44, 069101 (2020)]
54. D. Bhatia, S. Chakraborty, A. Dighe, JHEP **03**, 117 (2017). DOI 10.1007/JHEP03(2017)117
55. K. Fuyuto, H.L. Li, J.H. Yu, Phys. Rev. D **97**(11), 115003 (2018). DOI 10.1103/PhysRevD.97.115003

56. L. Bian, H.M. Lee, C.B. Park, *Eur. Phys. J. C* **78**(4), 306 (2018). DOI 10.1140/epjc/s10052-018-5777-1
57. S.F. King, *JHEP* **09**, 069 (2018). DOI 10.1007/JHEP09(2018)069
58. G.H. Duan, X. Fan, M. Frank, C. Han, J.M. Yang, *Phys. Lett. B* **789**, 54 (2019). DOI 10.1016/j.physletb.2018.12.005
59. Z. Kang, Y. Shigekami, *JHEP* **11**, 049 (2019). DOI 10.1007/JHEP11(2019)049
60. L. Calibbi, A. Crivellin, F. Kirk, C.A. Manzari, L. Vernazza, *Phys. Rev. D* **101**(9), 095003 (2020). DOI 10.1103/PhysRevD.101.095003
61. W. Altmannshofer, J. Davighi, M. Nardecchia, *Phys. Rev. D* **101**(1), 015004 (2020). DOI 10.1103/PhysRevD.101.015004
62. B. Capdevila, A. Crivellin, C.A. Manzari, M. Montull, *Phys. Rev. D* **103**(1), 015032 (2021). DOI 10.1103/PhysRevD.103.015032
63. A.M. Sirunyan, et al., (2021)
64. G. Aad, et al., *Phys. Lett. B* **796**, 68 (2019). DOI 10.1016/j.physletb.2019.07.016
65. B.C. Allanach, J.M. Butterworth, T. Corbett, *JHEP* **08**, 106 (2019). DOI 10.1007/JHEP08(2019)106
66. J. Davighi, Topological effects in particle physics phenomenology. Ph.D. thesis, Cambridge U., DAMTP (2020). DOI 10.17863/CAM.47560
67. J. Aebischer, J. Kumar, P. Stangl, D.M. Straub, *Eur. Phys. J. C* **79**(6), 509 (2019). DOI 10.1140/epjc/s10052-019-6977-z
68. A. Pomarol, D. Tommasini, *Nucl. Phys. B* **466**, 3 (1996). DOI 10.1016/0550-3213(96)00074-0
69. R. Barbieri, G.R. Dvali, L.J. Hall, *Phys. Lett. B* **377**, 76 (1996). DOI 10.1016/0370-2693(96)00318-8
70. R. Barbieri, G. Isidori, J. Jones-Perez, P. Lodone, D.M. Straub, *Eur. Phys. J. C* **71**, 1725 (2011). DOI 10.1140/epjc/s10052-011-1725-z
71. G. Blankenburg, G. Isidori, J. Jones-Perez, *Eur. Phys. J. C* **72**, 2126 (2012). DOI 10.1140/epjc/s10052-012-2126-7
72. R. Barbieri, D. Buttazzo, F. Sala, D.M. Straub, *JHEP* **07**, 181 (2012). DOI 10.1007/JHEP07(2012)181
73. J. Davighi, arXiv:2105.06918 (2021)
74. P. Zyla, et al., *PTEP* **2020**(8), 083C01 (2020). DOI 10.1093/ptep/ptaa104
75. W. Buchmüller, D. Wyler, *Nucl. Phys.* **B268**, 621 (1986). DOI 10.1016/0550-3213(86)90262-2
76. I. Brivio, M. Trott, *Phys. Rept.* **793**, 1 (2019). DOI 10.1016/j.physrep.2018.11.002
77. A. Dedes, W. Materkowska, M. Paraskevas, J. Rosiek, K. Suxho, *JHEP* **06**, 143 (2017). DOI 10.1007/JHEP06(2017)143
78. B. Grzadkowski, M. Iskrzynski, M. Misiak, J. Rosiek, *JHEP* **10**, 085 (2010). DOI 10.1007/JHEP10(2010)085
79. D.M. Straub, (2018)
80. J. Aebischer, J. Kumar, D.M. Straub, *Eur. Phys. J. C* **78**(12), 1026 (2018). DOI 10.1140/epjc/s10052-018-6492-7
81. J. Aebischer, et al., *Comput. Phys. Commun.* **232**, 71 (2018). DOI 10.1016/j.cpc.2018.05.022
82. S. Schael, et al., *Phys. Rept.* **427**, 257 (2006). DOI 10.1016/j.physrep.2005.12.006
83. W. Altmannshofer, P. Stangl, (2021)
84. A. Bazavov, et al., *Phys. Rev. D* **93**(11), 113016 (2016). DOI 10.1103/PhysRevD.93.113016
85. L. Di Luzio, M. Kirk, A. Lenz, *Phys. Rev. D* **97**(9), 095035 (2018). DOI 10.1103/PhysRevD.97.095035
86. D. King, A. Lenz, T. Rauh, *JHEP* **05**, 034 (2019). DOI 10.1007/JHEP05(2019)034
87. J. Matias, F. Mescia, M. Ramon, J. Virto, *JHEP* **04**, 104 (2012). DOI 10.1007/JHEP04(2012)104
88. S. Descotes-Genon, L. Hofer, J. Matias, J. Virto, *JHEP* **06**, 092 (2016). DOI 10.1007/JHEP06(2016)092
89. J.E. Camargo-Molina, A. Celis, D.A. Faroughy, *Phys. Lett. B* **784**, 284 (2018). DOI 10.1016/j.physletb.2018.07.051
90. L. Alasfar, A. Azatov, J. de Blas, A. Paul, M. Valli, *JHEP* **12**, 016 (2020). DOI 10.1007/JHEP12(2020)016
91. D. Bećirević, O. Sumensari, *JHEP* **08**, 104 (2017). DOI 10.1007/JHEP08(2017)104
92. R. Coy, M. Frigerio, F. Mescia, O. Sumensari, *Eur. Phys. J. C* **80**(1), 52 (2020). DOI 10.1140/epjc/s10052-019-7581-y
93. W. Altmannshofer, et al., *PTEP* **2019**(12), 123C01 (2019). DOI 10.1093/ptep/ptz106. [Erratum: *PTEP* 2020, 029201 (2020)]